EOS, TRANSACTIONS, AMERICAN GEOPHYSICAL UNION

VOLUME 91 NUMBER 16
20 APRIL 2010
PAGES 141–152

Reconciling Differing Views of Tropical Pacific Climate Change

PAGES 141–142

Recent analyses of global warming projections simulated with global climate models (GCMs) suggest that the tropical Pacific does not become El Niño– or La Niña–like in response to increased greenhouse gases (GHGs). Rather, the physical mechanisms that drive tropical Pacific climate change depart substantially from the El Niño–Southern Oscillation (ENSO) analogy often invoked for interpreting future climate changes [e.g., *Knutson and Manabe,* 1995; *Meehl and Washington,* 1996; *Cane et al.,* 1997; *Collins et al.,* 2005; *Meehl et al.,* 2007; *Lu et al.,* 2008; *Cox et al.,* 2004] and past climate changes [e.g. *Lea et al.,* 2001; *Koutavas et al.,* 2002]. This presents an opportunity for reconciling theory, models, and observations.

An ENSO analogy typically is invoked for interpreting tropical Pacific climate change because if an external forcing introduces some east-west asymmetry, this asymmetry can be amplified in the same way as interannual perturbations are, through the positive ocean-atmosphere Bjerknes feedback. This then would lead to an altered mean state of the tropical Pacific resembling El Niño or La Niña [*Dijkstra and Neelin,* 1995]. For instance, the model projections used for the Intergovernmental Panel on Climate Change (IPCC) Fourth Assessment Report (AR4) anticipate tropical Pacific climate change in response to increased GHGs that has been described as El Niño–like [*Meehl et al.,* 2007]. These models project robust enhanced equatorial warming [*Liu et al.,* 2006; *DiNezio et al.,* 2009] and a weakening of the overturning atmosphere circulation across the tropical Pacific, i.e., the Walker circulation [*Vecchi and Soden,* 2007], both of which occur during El Niño events. However, these experiments also show a shoaling and sharpening of the equatorial thermocline [*Vecchi and Soden,* 2007; *DiNezio et al.,* 2009] (Figure 1a). This is in contrast to El Niño events, when the thermocline response is heavily dominated by a relaxed tilt (Figure 1b).

By P. DiNezio, A. Clement, and G. A. Vecchi

The projected changes in thermocline depth are consistent with the equilibrium response to weaker trade winds, consisting of a zonal mean shoaling of the thermocline in response to the curl of the wind, in addition to the relaxation of the thermocline tilt [*Cane and Sarachik,* 1981; *Clarke,* 2010]. In the eastern equatorial Pacific, the zonal mean shoaling of the thermocline opposes the deepening due to a relaxed tilt, thereby limiting the coupling between changes in winds and sea surface temperature (SST). In addition to this response, increased thermal stratification enhances ocean dynamical cooling [*DiNezio et al.*, 2009] in the eastern basin, putting a brake on SST growth. The increased stratification can be attributed to weaker warming in the subtropical oceans [i.e., *Seager and Murtugudde,* 1997]; however, these mechanisms have not been extensively explored in controlled numerical experiments with IPCC-class coupled GCMs. Because of the weaker Bjerknes feedback, atmospheric feedbacks appear to influence only SST locally [*DiNezio et al.,* 2009] and east-west asymmetries are not amplified. Nonetheless, the response in atmospheric feedbacks can lead to substantial intermodel differences in the SST response. Evaluation and improvement of the representation of cloud feedbacks are needed for model convergence.

Controls on the Walker Circulation

A second difference is that under global warming, the Walker circulation weakens due to changes in the hydrological cycle extending beyond the equatorial Pacific [*Held and Soden,* 2006; *Vecchi and Soden,* 2007] that are not necessarily related to the zonal SST gradient. This mechanism explains why the majority of the IPCC AR4 models simulate a weakening of the zonal sea level pressure (SLP) gradient [*Vecchi and Soden,* 2007] accompanied by either a strengthened or a weakened zonal SST gradient depending on the model (see Figure S1 in the electronic supplement to this *Eos* issue (http://www.agu.org/eos_elec/)).

Though some questions about the true sensitivity of the hydrological cycle to greenhouse forcing remain [*Wentz et al.,* 2007], it is clear that there are other constraints on the strength of the Walker circulation beyond the zonal SST gradient; hence, a weakened SLP gradient does not necessarily rule out a strengthened SST gradient.

Reconciling SST and SLP Observations

These concepts have implications for interpreting observations. The few available data sets suggest a reduction of about 5% in the zonal SLP gradient [*Vecchi et al.,* 2006; *Bunge and Clarke,* 2009] and a zonal mean shoaling and relaxation of the thermocline tilt [*Vecchi et al.,* 2006; *Zhang et al.,* 2008]. However, there has been much debate as to the observed change in SST gradient [Cane et al., 1997; Vecchi et al., 2008] because the different SST reconstructions do not agree in the sign of the east-west gradient changes for the twentieth century, even during the satellite era [Vecchi et al., 2008]. According to the climate models, though, any of the SST reconstructions could be physically consistent with the observed changes in SLP (see Figure S1 in the electronic supplement) when the ENSO analogy is relaxed.

An evaluation of trends in the SST observations used to derive these reconstructions is needed to resolve the disagreement. For instance, an analysis of SST data suggests warming over the eastern equatorial Pacific during the twentieth century [*Bunge and Clarke,* 2009], ruling out the cooling trend suggested by the Hadley Centre sea ice and sea surface temperature data set (HadISST). However, more details on the spatial pattern of the SST trends are needed to test the enhanced equatorial warming hypothesis.

The distinction between global warming and ENSO is even more significant in the response of precipitation and extratropical atmospheric circulation. GCMs project a weakening and poleward expansion of the Hadley circulation and a poleward shift of the subtropical jet in response to increased GHGs. In contrast, during El Niño, the Hadley circulation strengthens and the jets shift equatorward [*Lu et al.,* 2008]. For instance, GCMs project a drier southwestern North America [*Seager et al.,* 2007], a region that gets more precipitation during El Niño years.

In general, the response of the hydrological cycle to global warming (Figure 1c) is best characterized by wet regions becoming wetter and dry regions becoming drier [*Held and Soden,* 2006] instead of El Niño–like (Figure 1d). Moreover, since Indonesia dries during El Niño years, more frequent forest fires would be expected as the planet warms [*Field et al.,* 2009]; however, the majority of the models project increased precipitation. Similarly, increased precipitation is projected for the monsoon regions of Asia, where droughts occur during El Niño. The projections for Amazonia are especially interesting since a previous GCM experiment has suggested a severe drying of the Amazon rain forest associated with an El Niño–like response in the equatorial Pacific [*Cox et al.,* 2004]. This catastrophic scenario cannot be ruled out because the experiment included an interactive carbon cycle.

However, theory and GCMs indicate that the equatorial thermocline has a strong negative feedback on global warming time scales, balancing this and other positive feedbacks and preventing the equatorial Pacific from becoming El Niño–like. An assessment of the sensitivity of these feedbacks is needed to reliably project the response of the tropics to increased GHGs.

This understanding of the mechanisms of future tropical Pacific climate change also can be applied to reconstructions of the climate of the Last Glacial Maximum (~20,000 years ago), where El Niño and La Niña analogies have been made. Proxies based on analysis of foraminifera suggest a stronger zonal SST gradient [*McIntyre,* 1981] and a stronger thermocline tilt [*Andreasen and Ravelo*, 1997]; magnesium/calcium ratios in foraminifera suggest either a weaker [*Koutavas et al.*, 2002] or unaltered [*Otto-Bliesner et al.,* 2009] zonal SST gradient; while models simulate the full range of increased to decreased SST gradients [*Otto-Bliesner et al.,* 2009]. However, all models simulate a deeper thermocline and a stronger Walker circulation, which, according to the arguments of *Vecchi and Soden* [2007], could result from global cooling. Hence, as in the case of global warming, there can be significant ocean and atmospheric changes without robust changes in the zonal SST gradient. From these arguments, it is clear that proxies of the thermocline or trade wind strength would be better suited than the zonal SST gradient to constrain the understanding of the physical processes operating in the Last Glacial Maximum tropics.

To summarize, recent theoretical, modeling, and observational evidence suggests that the physical processes operating during tropical Pacific climate change allow for a less rigid relationship among SSTs, the thermocline, and trade winds than that resulting from the Bjerknes feedback. These studies indicate that the fundamental ocean dynamics that govern the thermocline response limit the amplification of east-west asymmetries, providing a plausible explanation for the lack of robust evidence of El Niño–like warming in observations despite an observed weakening of the Walker circulation. Moreover, according to GCM projections, the associated precipitation impacts in response to greenhouse forcing are not El Niño–like. As such, adherence to an ENSO analogy for interpreting tropical Pacific climate change can lead to serious misconceptions.

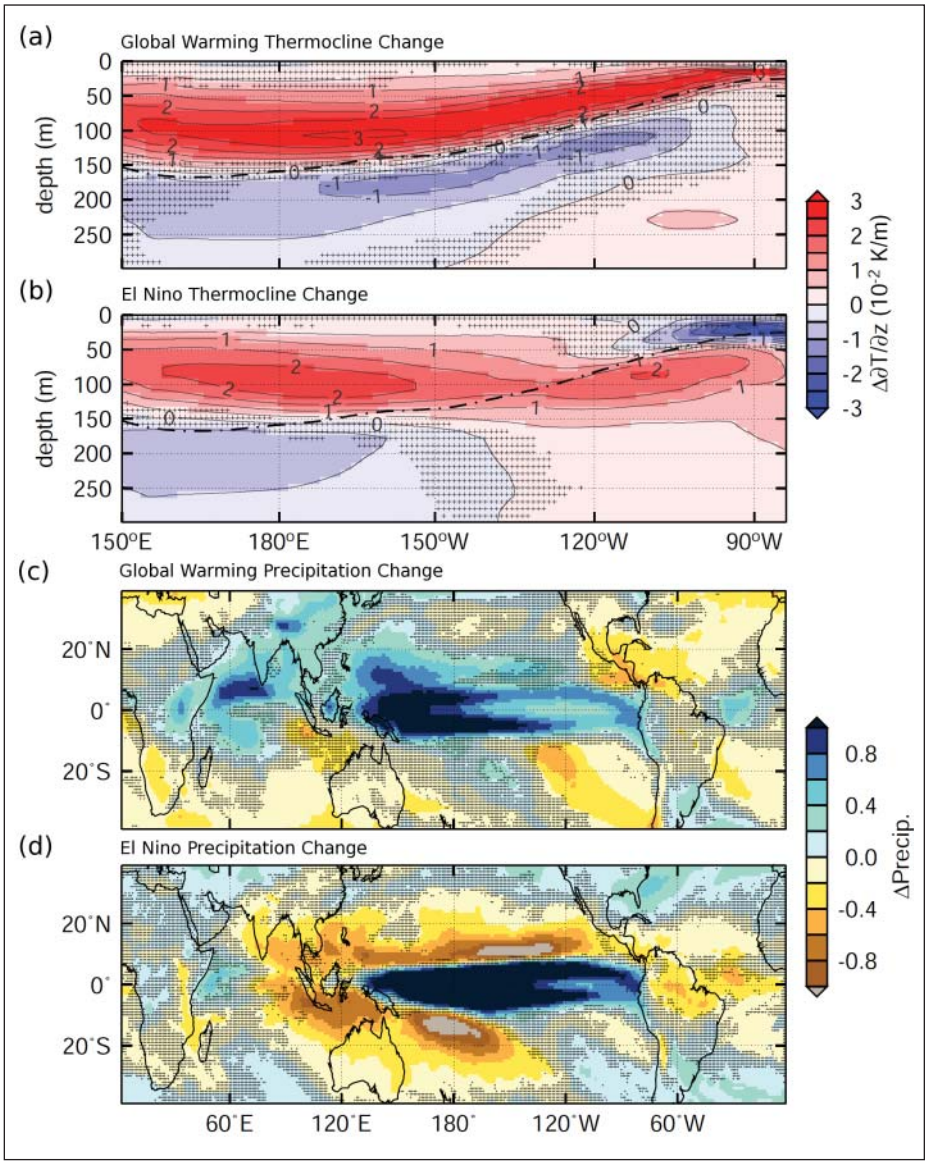

Fig. 1. (a) Multimodel change in vertical temperature gradient simulated by 21 general circulation models (GCMs) in experiments under emission scenario A1B of the Intergovernmental Panel on Climate Change Special Report on Emissions Scenarios *[*Nakicenovic et al., *2000]. This emissions scenario considers future economic development with balanced emphasis on all energy sources with carbon dioxide (CO_2) concentrations stabilizing at 720 parts per million after year 2100. (b) Multimodel anomaly in vertical temperature gradient averaged from composite El Niño events simulated by each of the 21 GCMs in experiments with forcing corresponding to the twentieth-century experiment (20C3M). Figures 1a and 1b depict an equatorial band between 5°S and 5°N. For Figures 1a and 1b, the dash-dotted line is the depth of the multimodel maximum vertical temperature gradient (i.e., the thermocline) in the control experiment (20C3M). (c) Multimodel change in precipitation simulated by 21 GCMs in response to increased CO_2 simulated in the SRESA1B experiment. (d) Multimodel precipitation anomaly averaged from composite El Niño events simulated by each of the 21 GCMs in the 20C3M experiment. In Figures 1a–1d, stippling indicates where fewer than 15 models simulate a response with the same sign as the multimodel mean response.*

Acknowledgments

We acknowledge the various international modeling groups participating in Coupled Model Intercomparison Project Phase 3 (CMIP3) and Paleoclimate Modelling Intercomparison Phase 2 (PMIP2). We are grateful for comments from B. Kirtman, M. Cane, M. Collins, and one anonymous reviewer, who helped improve the manuscript. The U.S. National Science

Foundation (grant 0500275) and U.S. National Oceanic and Atmospheric Administration (grant NA0604310142) supported this work.

References

Andreasen, D. J., and A. C. Ravelo (1997), Tropical Pacific Ocean thermocline depth reconstructions for the Last Glacial Maximum, *Paleoceanography, 12*(3), 395–413.

Bunge, L., and A. J. Clarke (2009), A verified estimation of the El Niño index NINO3.4 since 1877, *J. Clim., 22,* 3979–3992.

Cane, M. A., and E. S. Sarachik (1981), The response of a linear baroclinic equatorial ocean to periodic forcing, *J. Mar. Res., 39*(4), 651–693.

Cane, M. A., A. C. Clement, A. Kaplan, Y. Kushnir, D. Pozdnyakov, R. Seager, S. E. Zebiak, and R. Murtugudde (1997), Twentieth century sea surface temperature trends, *Science, 275,* 957–960.

Clarke, A. J. (2010), Analytical theory for the quasi-steady and low-frequency equatorial ocean response to wind forcing: The "tilt" and "warm water volume" modes, *J. Phys. Oceanogr., 40*(1), 121–137.

Collins, M., et al. (2005), El Niño– or La Niña–like climate change?, *Clim. Dyn., 24*(1), 89–104.

Cox, P. M., R. A. Betts, M. Collins, P. P. Harris, C. Huntingford, and C. D. Jones (2004), Amazonian forest dieback under climate-carbon cycle projections for the 21st century, *Theor. Appl. Climatol., 78,* 137–156.

Dijkstra, H. A., and J. D. Neelin (1995), Ocean-atmosphere interaction and the tropical climatology: part II. Why the Pacific cold tongue is in the east, *J. Clim., 8,* 1343–1359.

DiNezio, P., A. Clement, G. A. Vecchi, B. J. Soden, B. Kirtman, and S.-K. Lee (2009), Climate response of the equatorial Pacific to global warming, *J. Clim., 22,* 4873–4892.

Field, R. D., G. R. van der Werf, and S. S. P. Shen (2009), Human amplification of drought-induced biomass burning in Indonesia since 1960, *Nat. Geosci., 2,* 185–188, doi:10.1038/ngeo443.

Held, I. M., and B. J. Soden (2006), Robust responses of the hydrological cycle to global warming, *J. Clim., 19,* 5686–5699.

Knutson, T. R., and S. Manabe (1995), Time-mean response over the tropical Pacific to increased CO_2 in a coupled ocean-atmosphere model, *J. Clim., 8,* 2181–2199.

Koutavas, A., J. Lynch-Stieglitz, T. M. Marchitto, and J. P. Sachs (2002), El Niño–like pattern in ice age tropical Pacific sea surface temperature, *Science, 297,* 226–230.

Lea, D. W., D. K. Pak, and H. J. Spero (2001), Climate impact of late Quaternary equatorial Pacific sea surface temperature variations, *Science, 289,* 1719–1724.

Liu, Z., S. J. Vavrus, F. He, N. Wen, and Y. Zhang (2006), Rethinking tropical ocean response to global warming: The enhanced equatorial warming, *J. Clim., 18,* 4684–4700.

Lu, J., G. Chen, and D. M. W. Frierson (2008), Response of the zonal mean atmospheric circulation to El Niño versus global warming, *J. Clim., 21,* 5835–5851.

McIntyre, A., et al. (1981), Seasonal reconstructions of the Earth's surface at the Last Glacial Maximum, *Geol. Soc. Am. Map Chart Ser., MC-36,* 9 pp.

Meehl, G. A., and W. M. Washington (1996), El Niño–like climate change in a model with increased atmospheric CO_2 concentrations, *Nature, 382,* 56–60.

Meehl, G. A., et al. (2007), Global climate projections, in *Climate Change 2007: The Physical Science Basis—Contribution of Working Group I to the Fourth Assessment Report of the Intergovernmental Panel on Climate Change,* pp. 747–845, Cambridge Univ. Press, New York.

Nakicenovic, N., et al. [2000], *Intergovernmental Panel on Climate Change Special Report on Emissions Scenarios*, Cambridge Univ. Press, New York.

Otto-Bliesner, B. L., et al. (2009), A comparison of PMIP2 model simulations and the MARGO proxy reconstruction for tropical sea surface temperatures at Last Glacial Maximum, *Clim. Dyn., 32*(6), 799–815, doi:10.1007/s00382-008-0509-0.

Seager, R., and R. Murtugudde (1997), Ocean dynamics, thermocline adjustment and regulation of tropical SST, *J. Clim., 10,* 521–539.

Seager, R., et al. (2007), Model projections of an imminent transition to a more arid climate in southwestern North America, *Science, 316*(5828), 1181–1184.

Vecchi, G. A., and B. J. Soden (2007), Global warming and the weakening of the tropical circulation, *J. Clim., 20,* 4316–4340.

Vecchi, G. A., B. J. Soden, A. T. Wittenberg, I. M. Held, A. Leetmaa, and M. J. Harrison (2006), Weakening of tropical Pacific atmospheric circulation due to anthropogenic forcing, *Nature, 441,* 73–76.

Vecchi, G. A., A. Clement, and B. J. Soden (2008), Examining the tropical Pacific's response to global warming, *Eos Trans. AGU, 89*(9), 81, 83.

Wentz, F. J., L. Ricciardulli, K. Hilburn, and C. Mears (2007), How much more rain will global warming bring?, *Science, 317,* 233–235.

Zhang, Q., Y. Guan, and H. Yang (2008), ENSO amplitude change in observation and coupled models, *Adv. Atmos. Sci., 25,* 361–366.

Author Information

Pedro DiNezio, Cooperative Institute for Marine and Atmospheric Studies, University of Miami, Miami, Fla.; E-mail: pdinezio@rsmas.miami.edu; Amy Clement, Rosenstiel School of Marine and Atmospheric Science, University of Miami; and Gabriel Vecchi, Geophysical Fluid Dynamics Laboratory, National Oceanic and Atmospheric Administration, Princeton, N. J.

NEWS

In Brief

PAGE 142

Volcanic vents found in deep Caribbean waters Scientists surveying the Cayman Trough in the Caribbean Sea have discovered the world's deepest undersea volcanic vents, or "black smokers," the National Oceanography Center (NOC) in Southampton, UK, announced on 11 April. The vents were found at a depth of 5000 meters, about 800 meters deeper than any previously discovered.

Jon Copley, a marine biologist at the University of Southampton's School of Ocean and Earth Science, said, "Seeing the world's deepest black-smoker vents looming out of the darkness was awe-inspiring." Geochemist Doug Connelly of NOC, principal scientist of the expedition, noted, "We hope our discovery will yield new insights into biogeochemically important elements in one of the most extreme naturally occurring environments on our planet." Researchers used an NOC-developed Autosub6000 robot submarine, which was remotely controlled from the Royal Research Ship *James Cook*. For more information, visit http://www.thesearethevoyages.net/.

Updated International Geomagnetic Reference Field The latest release of International Geomagnetic Reference Field (IGRF-11) was published online at the end of 2009. IGRF is a standard reference model of Earth's internal magnetic field. The reference field is typically updated every 5 years by an international team of geomagnetic field modelers working under the auspices of the International Association of Geomagnetism and Aeronomy and in collaboration with institutions collecting and disseminating magnetic field measurements from satellites and a worldwide network of ground-based observatories.

As with earlier versions of the reference field, IGRF-11 provides a global picture of the past and present geomagnetic field as well as a linear prediction of field changes over the upcoming 5 years. IGRF is widely used in navigation and heading systems, geophysical surveying, and space weather modeling and prediction. For more information and to download the new IGRF-11 model, visit the Web site http://www.ngdc.noaa.gov/IAGA/vmod/igrf.html.

—RANDY SHOWSTACK, Staff Writer